PNAS RESEARCH ARTICLE | GENETICS

Two differentially stable rDNA loci coexist on the same chromosome and form a single nucleolus

Luciana Lazar-Stefanita[a,b], Jingchuan Luo[a,b,1], Max A. B. Haase[a,b,c], Weimin Zhang[a,b], and Jef D. Boeke[a,b,d,2]

Contributed by Jef D. Boeke; received November 15, 2022; accepted January 20, 2023; reviewed by Jeffrey S. Smith and Kenneth H. Wolfe

The nucleolus is the most prominent membraneless compartment within the nucleus—dedicated to the metabolism of ribosomal RNA. Nucleoli are composed of hundreds of ribosomal DNA (rDNA) repeated genes that form large chromosomal clusters, whose high recombination rates can cause nucleolar dysfunction and promote genome instability. Intriguingly, the evolving architecture of eukaryotic genomes appears to have favored two strategic rDNA locations—where a single locus per chromosome is situated either near the centromere (*CEN*) or the telomere. Here, we deployed an innovative genome engineering approach to cut and paste to an ectopic chromosomal location—the ~1.5 mega-base rDNA locus in a single step using CRISPR technology. This "megablock" rDNA engineering was performed in a fused-karyotype strain of *Saccharomyces cerevisiae*. The strategic repositioning of this locus within the megachromosome allowed experimentally mimicking and monitoring the outcome of an rDNA migratory event, in which twin rDNA loci coexist on the same chromosomal arm. We showed that the twin-rDNA yeast readily adapts, exhibiting wild-type growth and maintaining rRNA homeostasis, and that the twin loci form a single nucleolus throughout the cell cycle. Unexpectedly, the size of each rDNA array appears to depend on its position relative to the *CEN*, in that the locus that is *CEN*-distal undergoes size reduction at a higher frequency compared to the *CEN*-proximal counterpart. Finally, we provided molecular evidence supporting a mechanism called paralogous *cis*-rDNA interference, which potentially explains why placing two identical repeated arrays on the same chromosome may negatively affect their function and structural stability.

megablock chromosome engineering | Hi-C maps | *cis* duplicated rDNA loci | nucleolus

Significance

Our work outlines an innovative approach to chromosome engineering that allowed a single-step relocation of over 1 megabase of DNA using CRISPR on a fused megachromosome in yeast. We deployed this technology to manipulate the position of the rDNA locus in an unprecedented configuration, wherein "twin" loci coexist on the same chromosomal arm, that reveals: i) exquisite rRNA homeostasis, unperturbed by the rDNA gene surplus, ii) dependency of rDNA-array stability on chromosome position, where their differential decay suggests an evolutionary preference for a centromere-proximal locus, and iii) that they form a single nucleolus. Overall, our work sheds light on the structural evolution of rDNA loci and provides tools to study the rDNA dosage effect on cellular metabolism.

The most abundant genes in cells are those encoding ribosomal RNA (rRNA), usually arranged as a series of tandem repeats that include transcriptional units for rRNAs spaced by nontranscribed sequences (1–3). As rRNAs are the structural components of ribosomes, they represent the most abundant RNA molecules in most organisms, accounting for 60 to 70% of cellular transcripts, e.g., 10^5/yeast cell (4) and 10^{6-7}/animal cell (5).

In eukaryotes, rRNA transcription and ribosome assembly take place in a membraneless organelle that occupies a substantial proportion of the cell nucleus, namely the nucleolus (6, 7). The incongruous features of the nucleolus—such as rapid molecular turnover and phase-separation–like dynamics, yet maintenance of a coherent shape—are reconciled by two distinct but complementary models: namely liquid–liquid phase separation (LLPS) (5, 8) and polymer–polymer phase separation (PPPS) (9), the latter of which proposes that rRNA and associated proteins self-organize into membraneless condensates based on intrinsic biophysical properties (10, 11). Moreover, the structure and activity of the nucleolus are features that are highly dynamic throughout cell division, as is evident in eukaryotes with open mitosis in which nucleolar breakdown and transcriptional shutdown are concomitant with entry into mitosis (12, 13). The nucleoli assemble around distinct chromosomal clusters/loci, gathering hundreds of tandemly repeated ribosomalDNA (rDNA) genes that largely exceed the number of units needed for survival. Indeed, typically, only ~50% of the rDNA genes are actively transcribed while the remainder are kept inactive, an equilibrium that can be tuned by altering the total copy number of ribosomal genes at this locus (14, 15). Therefore, a high rRNA level—correlated with growth rate in many microbes (16)—can be achieved not only by boosting transcription but also by rDNA copy number expansion (17–19). Given their repetitive nature and the high demand for rRNA transcripts, the rDNA loci are among the most unstable genome structures (20, 21). Their instability relies on a repeat-mediated homologous recombination mechanism that requires both rDNA replication (17, 18) and transcriptional processes (19, 22), which often lead to clonal variation in the repeat number and size of the locus.

Cyto-taxonomic studies, based on the widespread usage of fluorescence in situ hybridization, enabled mapping of rDNA loci on chromosomes of thousands of species. The number and position of these loci, each containing hundreds of tandem repeats, were

Reviewers: J.S.S., University of Virginia; and K.H.W., University College Dublin.

Competing interest statement: The authors have organizational affiliations to disclose: J.D.B. is a Founder and Director of CDI Labs, Inc., a Founder of Neochromosome, Inc, a Founder of and Consultant to ReOpen Diagnostics, and serves or served on the Scientific Advisory Board of the following: Logomix, Inc., Modern Meadow, Inc., Rome Therapeutics, Inc., Sample6, Inc., Sangamo, Inc., Tessera Therapeutics, inc., and the Wyss Institute. The remaining authors declare no competing interests. The authors have stock ownership to disclose: J.D.B. has substantive interest in CDI Labs, Neochromosome, and ReOpen Diagnostics.

[1]Present address: Whitehead Institute for Biomedical Research, Cambridge, MA 02142.

[2]To whom correspondence may be addressed. Email: jef.boeke@nyulangone.org.

This article contains supporting information online at https://www.pnas.org/lookup/suppl/doi:10.1073/pnas.2219126120/-/DCSupplemental.

Published February 23, 2023.

compiled and used for in silico analyses of their evolving structure in plants (23) and animals (24). Collectively, these studies revealed that most taxa have genomes with multiple rDNA loci, with an average number of only three to four loci per diploid genome, indicating that most organisms tend to maintain a moderately low number of loci. In plants, locus number was positively correlated with genome size, whereas in animals, no such correlation was observed. Surprisingly, although rDNA loci were identified at nearly any chromosomal position, they prevalently appear either pericentromeric or peritelomeric [in >75% of karyotypes (24)]. Genome-wide studies in mammals (25) and yeasts (26) provided evidence to support the hypothesis that rDNA arrays have changed their chromosomal position multiple times during evolution: in almost every case, the native array disappeared entirely from the ancestral site, leaving behind a small "intergenic scar" (26).

These insights hint at two potential aspects of rDNA evolution: i) a common ancestral mechanism through which this locus migrates within genomes and ii) a potentially deleterious effect associated with more than a single rDNA locus per chromosome arm (25, 26). Regarding the first hypothesis, we can only speculate that recombination between nonhomologous sequences and "non-reciprocal crossover" between repeats (27–29) may be responsible for the relocation of rDNA and its size, respectively. Here, we address the second hypothesis by monitoring the effects of a rDNA migration event in which the entire native megabase rDNA array was transplanted to an ectopic intrachromosomal location through a cut-and-paste mechanism.

Results

In budding yeast, such as *Saccharomyces cerevisiae*, the *RDN1* locus is approximately a 1.5-Mb region that contains 150 to 200 copies of a 9.1-kb unit and accounts for ~10% of the entire yeast genome (30). Each repeat encodes four genes: 5.8S, 25S, 18S, and 5S rRNAs transcribed by RNA polymerase I and III (15, 31). The entire array exists in single copy on the right arm of chromosome *XII*, located roughly 300 kb from *CEN12* and ~600 kb from *TEL12R* (2, 32), and forms a single crescent-shaped nucleolus apposed to the nuclear envelope (33) (Fig. 1*A*). Here, we built yeast strains with multiple rDNA loci by mating haploid strains carrying a single locus on heterologous (nonhomologous) chromosomes (chr *XII* and chr *III*) (34) followed by the sporulation (name of induced gametogenesis in yeast) of the resulting diploid. This allowed the isolation of a haploid strain carrying two rDNA clusters on heterologous chromosomes, whose size was validated through pulsed-field gel electrophoresis (PFGE) (*SI Appendix*, Fig. S1*A*). Fluorescent microscopy of the nucleolus showed that this strain displays a single nucleolar compartment (Fig. 1*B* and *SI Appendix*, Fig. S1*B*) and confirmed the work of Hult et al. (35) on a rDNA array split on two distinct chromosomes. These results led us to conclude that yeast (like many other eukaryotes) can readily adapt to live with multiple rDNA loci on different chromosomes. However, it leaves unanswered the question of whether the yeast genome can be engineered with multimegabase rDNA loci coexisting on the same chromosome.

rDNA Megablock Engineering: One-Step Transplantation of a Megabase Locus to a Target Position. To answer the above question, we used a karyotype-engineered yeast strain carrying three megabase-sized chromosomes ($n = 3$; with chromosomes *A*, *B*, and *C*) that have been previously generated through sequential subtelomere fusion events of the sixteen wild-type (WT) chromosomes (36). These genome reengineering steps gave rise to megachromosome *C* (5.5 Mb-long), that resulted in a dramatic change in the position of the rDNA locus relative to the nearest active centromere (*CEN*) (left drawing in Fig. 1*C*, the black arrowhead points to the rDNA distal position). Precisely stated, on chr *C*, the rDNA-*CEN* distance increased ninefold relative to the WT distance, reaching up to ~2.7 Mb, whereas its native position relative to the nearest (right arm) telomere (*TEL*) remained unchanged. Not only this "passive" migration of the locus to a distal location did not affect growth [see JL411 strain generated by Luo et al. (36)], but it also provided a chromosomal arm long enough to allow for an insertion of a second *CEN*-proximal locus in *cis* (right drawing in Fig. 1*C*, the black arrowhead points at the rDNA proximal position). Here, we developed a variation of the CRISPR-Cas9 editing approach to engineer megachromosomes that we call 'megablock engineering' (Fig. 1*C* and *Methods*), in which a megabase-sized segment of a chromosome is moved to a target location, potentially anywhere in the genome. Megablock engineering deploys two CRISPR guide RNAs that cut at the boundaries of the genomic DNA "block" to be relocated, and a third guide cutting at the target location. Additionally, three "linker DNAs" are provided: one that joins the native rDNA locus flanking ends together and two that join the left and right junctions of the target locus to the ends of the megablock (Fig. 1*C*). In this case, the entire megabase long rDNA locus was removed from its native *CEN*-distal location and relocated 2 Mb closer to the *CEN* of chr *C* (essentially a "cut, paste, and repair" approach). This extremely aggressive genome engineering maneuver was surprisingly efficient, with 6/41 colonies score by PCR genotyping showing evidence of successful megablock engineering. Hi-C was used to structurally validate the rDNA locus transplantation (Fig. 1*D*, black arrowheads point at the rDNA boundaries). One such strain (JL665), with *CEN* proximal rDNA, was then used for further analyses and experiments. Of note, the orientation of the transplanted rDNA array relative to the chromosome anatomy was maintained to ensure locus directionality (e.g., rDNA replication and transcription orientation occur *TEL*-to-*CEN* in both the JL665 strain and its JL411 parent with *CEN* proximal and distal rDNA loci, respectively). Successively, by mating "parental" and "transplanted" strains, with either *CEN*-distal or *CEN*-proximal rDNA, respectively, we generated a heterozygous diploid with two loci asymmetrically positioned on each homolog of megachromosome *C*. Finally, haploids with duplicated rDNA loci in *cis* were isolated by sporulation of this diploid strain and their integration junctions were PCR verified (*SI Appendix*, Fig. S1 *C* and *D*).

Effects of rDNA Duplication on Fitness. Whole-genome sequencing validated the duplication of the rDNA locus in the haploid strains (LS71 with twin rDNA loci) by estimating twice as many rDNA-mapping reads in 2xrDNA/chr*C* (Fig. 2*A*). Importantly, the newly formed rDNA junction sequences were confirmed and no chromosomal abnormalities, potentially caused by recombination events between the two colinear loci, were detected (*SI Appendix*, Fig. S2*A*). Not only did the 2xrDNA isolates lack obvious fitness defects (Fig. 2*B* and *SI Appendix*, Fig. S2*B*), but they rapidly adapted to the excess of rDNA repeats by fine-tuning the rRNA levels (Fig. 2*C* and *SI Appendix*, Fig. S2 *C* and *D*). In addition, a small number of genes were differentially expressed in the 2xrDNA vs. 1xrDNA strains when grown to mid/late log phase (Fig. 2*D* and Dataset S2) and represented a nonrandom coherent set of genes, and distinct from the DEGs found between the two parent strains with 1xrDNA (*SI Appendix*, Fig. S2*E*). Notably, genes involved in the metabolism of glucose and metal transport were down-regulated (*HXT1*, *CTR1*, *SIT1*, *FRE1*), whereas phosphate starvation-induced genes were up-regulated (*PHO84*, *PHO5*) in cells with 2xrDNA loci. Previous published work by Ju and Warner (37) reported that the transcription of

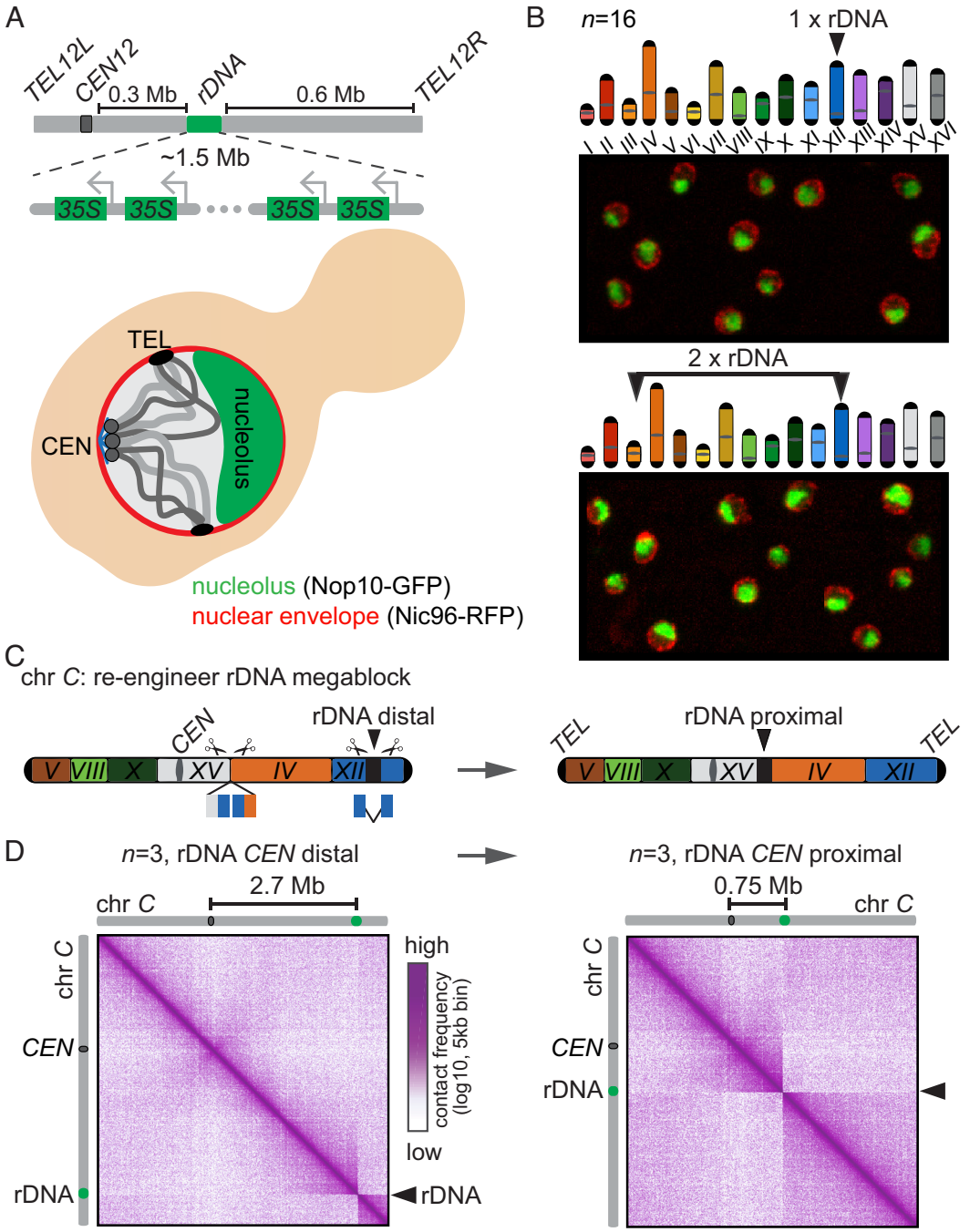

Fig. 1. Transplantation of the rDNA megablock to an ectopic genome location. (*A*) Diagram showing chromosome *XII* of wild-type yeast (*n* = 16, BY4741) that contains the rDNA locus (green), and below a simplified representation of nuclear organization in yeast, where examples of chromosome arms (gray lines) are anchored at the nuclear membrane through *CEN* and *TEL*, and the crescent-shaped nucleolus (green) consisting of rDNA genes. (*B*) Representative microscopy images of yeast nuclei with one or two rDNA loci (black arrowheads in the schematic indicate rDNA-containing chromosomes in WZ499 strain). (*C*) Schema illustrating the relocation (arrowheads) of the rDNA megablock (black box) on the fused megachromosome *C* (chr *C*: color code corresponds to the design of chromosome fusion) in *n* = 3 yeast strains (JL411 has a *CEN* distal rDNA locus, whereas, rDNA is *CEN* proximal in JL665). Colored blocks indicate sequence homology of the repair donors at CRISPR-Cas9 cutting sites. (*D*) Hi-C contact maps of chr *C* shown in gray on the *x* and *y* axes of each map. The rDNA locus is *CEN* distal on the *Left*, whereas, after transplantation, it appears *CEN* proximal on the *Right*. rDNA distances from the *CEN*s (dark gray) are indicated atop the maps.

ribosomal RNA precursors appears to be down-regulated even before yeast cultures enter mid-log growth, foreshadowing the diauxic shift. Therefore, our results suggest that twin-rDNA cells may experience a delayed metabolic diauxic shift from glucose fermentation (fast growth) to respiration (slow growth), or even lack/skip the shift altogether in response to early deprivation of one or more nutrients, which greatly precede growth arrest.

Links between the function and structure of the rDNA locus in yeast have been previously described and showed that a subset of the repeats are usually actively transcribed while the remainder are silenced (14, 38). Their transcription level was correlated with distinct chromatin states, defined by the association of the repeats with DNA-folding markers of either euchromatin [e.g., high-mobility group proteins, Hmo1 (39)] or heterochromatin [e.g., silencing complex, SIR (40)]. Here, we identified mild changes in the expression level of these chromatin modifiers: the rDNA-silencing factor (Sir2) was up-regulated, whereas the active rDNA copy-associated protein Hmo1 was down-regulated in 2xrDNA compared to 1xrDNA strains (*SI Appendix*, Fig. S2*F*). This transcriptional anticorrelation is consistent with an excess of repeats

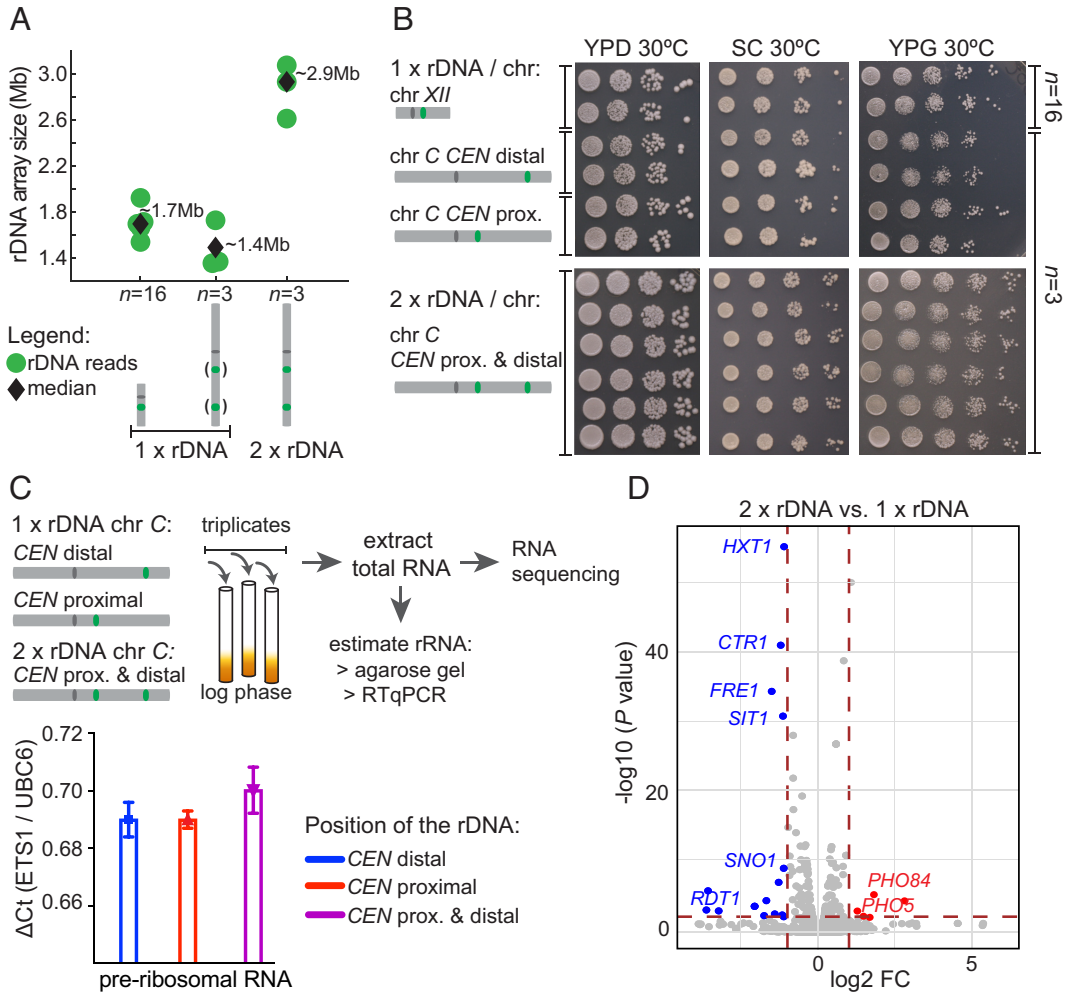

Fig. 2. Effects of rDNA duplication on cell fitness and transcriptomics. (*A*) Estimate of total length of the rDNA array by deep sequencing: % of rDNA aligned reads normalized by genome size (12.3 Mb). Schematics of chromosome *XII* (*n* = 16, BY4741) and megachromosome *C* (*n* = 3) are shown on the bottom of the plot (gray) and the position of the rDNA locus is highlighted in green. The parentheses indicate 1xrDNA locus per chromosome either *CEN* proximal or *CEN* distal (strains: JL411, JL665, and LS88); whereas, the configuration with 2xrDNA loci on chr *C* is shown without parentheses (independent isolates of LS71: C1 to C3). (*B*) Serial dilution assay on different growth conditions at 30 °C of *n* = 16 (BY4741) and *n* = 3 isolates with either single (JL411 and JL665) or duplicated rDNA (LS71). (*C*) Schematics of RNA-based assays in *n* = 3 isolates with 1xrDNA (JL411 and JL665) vs. 2xrDNA (LS71). RT-qPCR bar plot used to estimate changes in the synthesis of the ribosomal RNA precursor (ETS1) relative to the control messenger RNA, *UBC6*. (*D*) Volcano plot showing RNA-seq data comparing transcriptomes of 1xrDNA (JL411 and JL665) and 2xrDNA (LS71) strains in triplicates. Red and blue dots indicate differentially expressed genes in 2xrDNA vs. 1xrDNA: in blue down-regulated, in red up-regulated ($P < 10$ to 5, |fold change| > 2).

in twin-rDNA strains that may demand additional silencing. Next, we investigated the structural organization of chr *C* with twin-rDNA loci in *cis,* and their chromosomal (in)stability.

Structure of Chromosomes with twin-rDNA Loci in *cis*. We used Hi-C (41, 42) to probe the 3-dimensional structure of genomes with twin-rDNA arrays. The 2D (2 dimensional) contact maps of chr *C* of strains containing a single locus, either *CEN*-proximal or distal, were combined into a single control map (in other words, a bioinformatic merge of the two parental Hi-C maps into a single map followed by its normalization). For comparison purposes, the control 2D map (Fig. 3 *A*, *Bottom Left* triangle map) is displayed adjacent to that obtained from triplicate strains with *cis* twin-rDNA loci (Fig. 3 *A*, *Top Right* triangle map). In the control map, two nearly indistinguishable boundaries ("sharp" contact variations) formed at each rDNA location, as a result of similar insulation rates from their corresponding adjacent regions (outlined by blue squares, 1 and 2, in Fig. 3*A*). In contrast, the two boundaries in *cis* appeared to give rise to distinct contact frequencies (blue squares, 3 and 4, in Fig. 3*A*), where the insulation ("sharpness") at the *CEN* proximal rDNA cluster prevailed over the distal twin (the difference between the two rDNA boundaries in *cis* appears obvious in the contact ratio map in *SI Appendix*, Fig. S3*A*). This observed differential insulation at the two *cis* boundaries was validated through contact quantification plots for each locus that considered contacts between the intervening region enclosed by the two loci (1.9 Mb long) and the corresponding nonintervening, rDNA-flanking regions (highlighted by blue dashed rectangles on the Hi-C normalized maps (5 kb-binned) in Fig. 3*A*). From this analysis, we observed that the distal locus forms a weaker chromosome boundary (lower degree of insulation) when its *CEN*-proximal twin is located in *cis* (Fig. 3*B*), a result that suggested distinct levels of structural "bulkiness" between the *cis* rDNA loci.

Given that the 2xrDNA map represents consistent results obtained from three independent yeast isolates, we reasoned that the structural difference between the twin loci may arise from distinct epigenetic or genetic stability effects. Two major chromatin modifications at the distal locus could potentially be responsible for this divergence: i) increased heterochromatin through silencing that may result in a highly condensed/compacted structure, and/or ii) a reduction of rDNA repeat copy number at this

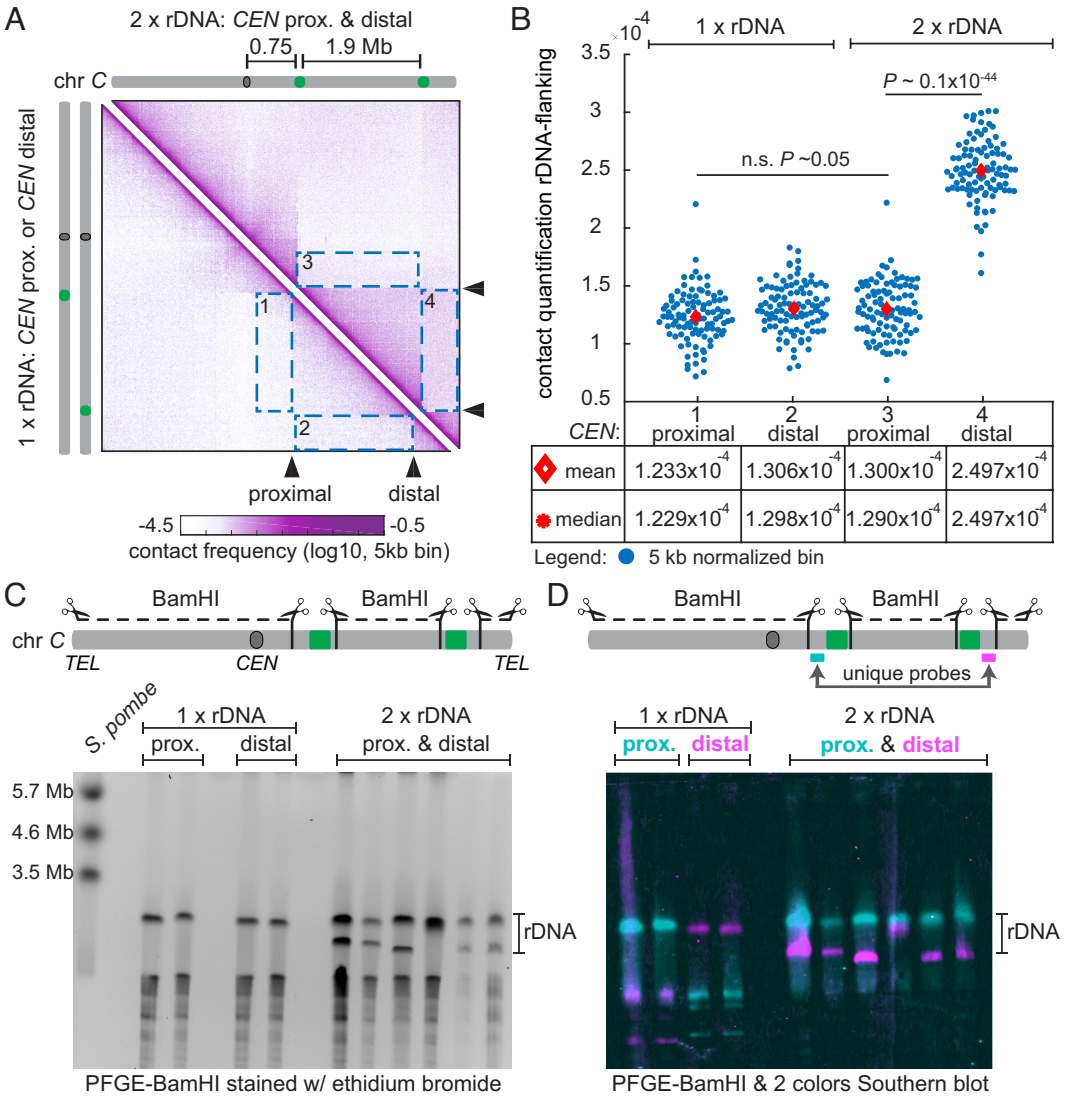

Fig. 3. Stability of the rDNA locus is a function of chromosome position. (*A*) Hi-C contact maps of megachromosome *C* (chr *C* in gray on the *x* and *y* axes of each contact map) in *n* = 3 strains with either one or two rDNA loci. *Bottom Left* triangle map: average representation of two merged contact maps with 1xrDNA on chr *C*, either *CEN* proximal (JL665) or *CEN* distal (JL411). *Top Right* map: average representation of three merged contact maps with 2xrDNA on chr *C CEN* proximal and distal (LS71 C1 to C3). rDNA distances from the *CEN* (dark gray) are indicated at the top of the map. (*B*) Quantifications of Hi-C contacts between the rDNA-flanking regions on chr *C* (500 kb long), highlighted in blue rectangles in panel *A* (rectangles 1 & 3 represent sequences upstream of the *CEN*-proximal rDNA boundary; whereas, 2 & 4 represent sequences downstream of the *CEN*-distal boundary), and the 1.9 Mb rDNA intervening sequence. Mean, median of absolute contact values, and their *P* values, calculated using the Kolmogorov–Smirnov test (K-S test), are indicated for each strain with one or two rDNA loci. (*C* and *D*) Estimate of rDNA array sizes. PFGE of BamHI-digested chromosomes (*C*) and the corresponding Southern blot with unique probes designed for each rDNA position (*D*). Each lane represents an independent isolate of *n* = 3 strains with 1xrDNA, either *CEN* proximal or *CEN* distal, or 2xrDNA in *cis CEN* proximal and distal. Schematic indicates the position of rDNA arrays and probes (cyan or fuchsia) on chr *C*. PFGE run specifications: *S. pombe* program for megasize chromosome separation.

distal locus. As the two loci have identical DNA sequences, we are unable to distinguish between rRNA transcripts originating from either locus; therefore, we cannot determine whether they are differentially expressed (*Discussion*). Even though we are unable to rule out the hypothesis of different levels of activity and/or silencing at the two *cis* rDNAs, their overall lengths can be directly measured to assess whether the two repeated arrays display differential stability rates. The size of each rDNA locus was estimated using PFGE and dual-color Southern blotting on BamHI-digested chromosomes (Fig. 3 *C* and *D* and *Methods*). After digestion with BamHI, which does not cut within the rDNA repeat unit, the rDNA loci were left with unique DNA-flanking sequences, that were used to design labeled DNA probes that specifically recognize each locus. Surprisingly, nearly all 2xrDNA independent isolates showed a consistent and locus-specific size reduction of the distal rDNA locus of ~500 to 700 kb when compared to the 1xrDNA-distal parent strain (Fig. 3*D*; PFGE control for chromosome preparation and PCR validations of each rDNA locus are shown in *SI Appendix*, Fig. S3 *B* and *C*). Also, we observed that the clonal variation in the size of the distal locus persisted in isolates passaged for ~100 generations (*SI Appendix*, Fig. S3*D*), suggesting that the excess rDNA genes are not detrimental in mitotically dividing cells in laboratory conditions. These results led us to conclude that rDNA repeats in yeast might be more stable when located *CEN*-proximal rather than distal. This is the evidence of a direct correlation between the stability of a repeated gene array and its relative chromosome location.

Finally, we probed the stability of the two loci in *cis* in the absence of Sir2, known to suppress recombination between repeated ribosomal genes (22, 40). We found that the two distinct rDNA bands were lost (replaced by a DNA smear) in all Δ*sir2* isolates (*SI Appendix*, Fig. S3*E*), supporting the idea that the size variation may depend on differential Sir2 activity at the two loci in *cis* that could cause distinct stability rates between them.

Mitotic Reorganization of the Nucleolus with *cis* rDNAs. For the nucleolus to be correctly segregated between mother and daughter cells, in late anaphase the rRNA transcription needs to be shut down to achieve rDNA-cluster condensation (43, 44). Importantly, the condensation process mainly involves the rDNA and is less pronounced across the remainder of the yeast genome.

Our previous work showed that the mitotic reorganization of chromatin is preserved along megachromosomes (45). Here, we specifically addressed the structure of megachromosome *C* with twin *cis* rDNAs and that of the resulting nucleolus during the cell cycle. Overall, we expected chr *C* to undergo a typical mitotic reorganization (46); however, it remained unknown how the ~1.9 Mb-long non-rDNA sequence linking the two loci may interfere with the structure of the nucleolus. Cells synchronized in G1 (alpha factor) and in anaphase [*cdc15-2* ts (47)] were imaged and showed very clearly that the two rDNAs consistently formed a single nucleolar mass per cell throughout mitosis (Fig. 4*A* and *SI Appendix*, Fig. S4*A*).

The Hi-C maps revealed yet another layer of structural complexity of the nucleolus. The G1 map displayed strong contacts between the two rDNAs in *cis*, but these were lost in late anaphase (Fig. 4*B*, black arrowhead; *SI Appendix*, Fig. S4*C*), suggesting that during anaphase the two loci are handled as single and independent chromosome units. Contact quantifications between the rDNA-flanking regions and the intervening region (as described in Fig. 3*B*) showed an overall decrease in anaphase compared to G1 (Fig. 4*C*), in agreement with their increased condensation during anaphase that may strengthen chromosome insulation at the two rDNA loci. Note that the folding status of the rDNA-intervening sequence on chr *C* is not influenced by the rDNA-flanking loci (*SI Appendix*, Fig. S4*B*, contact probability *p*(*s*) decay). Therefore, we conclude that i) the ~1.9 Mb rDNA-intervening sequence does not interfere with the formation of the 2xrDNA-nucleolus, and that ii) the two loci in *cis* are treated as independent chromosomal entities during anaphase condensation contrary to G1.

Discussion

Here, we provided the living evidence of a eukaryotic genome carrying more than one rDNA locus located within the same chromosomal arm. The remarkable stability of the yeast genome is highlighted in its transcriptomics and the homeostatic control of the rDNA repeats at each locus. The structure of the twin-rDNA nucleolus and its reorganization during cell cycle was

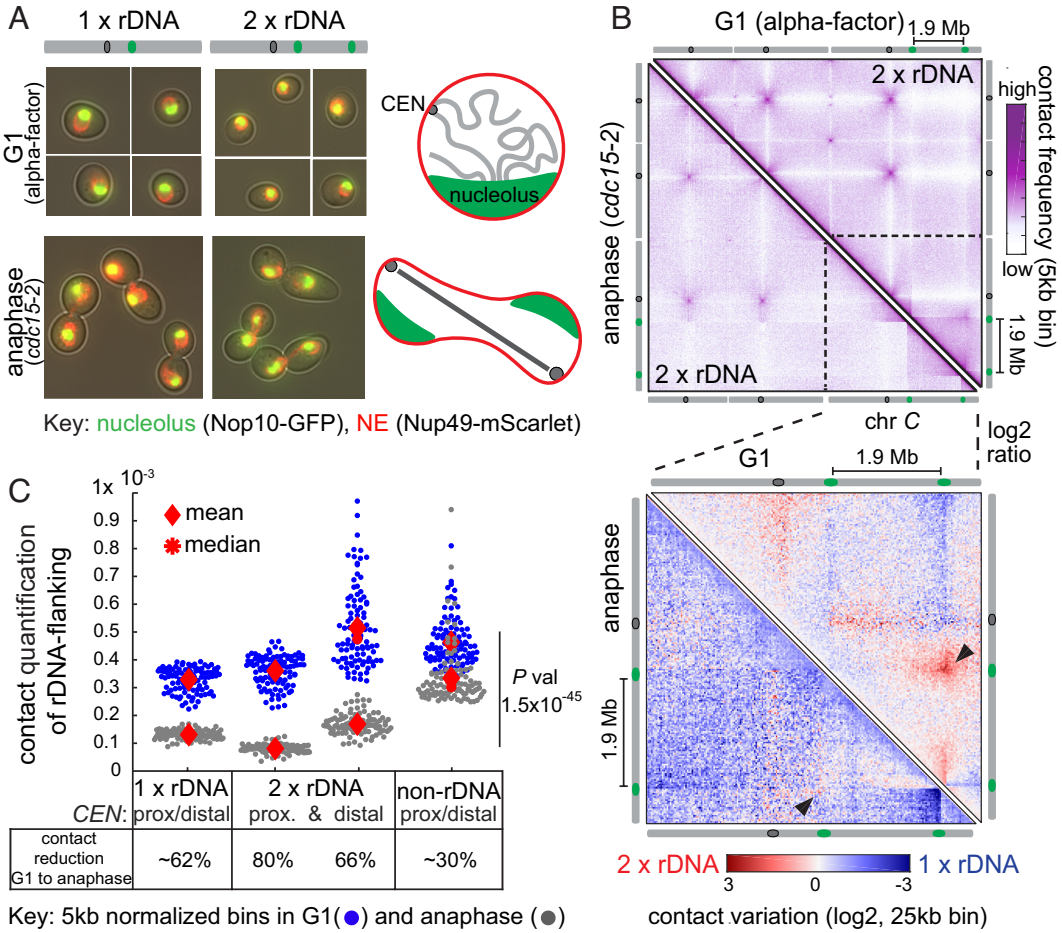

Fig. 4. Twin rDNA loci in *cis* form a single nucleolus during cell division. (*A*) Representative microscopy images of *n* = 3 strains with one rDNA locus (*CEN* proximal) or two loci in *cis* (*CEN* proximal and distal). Cells were synchronized in G1 (LS88 and LS90 strains grown in alpha factor at 25 °C) and late anaphase (LS95 and LS103 strains with *cdc15-2* ts mutation grown at 37 °C) before imaging. The insertion of white lines indicates that cells originated from different locations in the field of view. (*B*, *Top*) Hi-C maps of megachromosomes in *n* = 3, with two rDNA loci in *cis* on chr *C* (dashed outline), from cells synchronized in G1 (*Top Right* triangle map) and late anaphase (*Bottom Left* triangle map). *Bottom*: contact variation maps (log2-ratio) of chr *C* with 1xrDNA vs. 2xrDNA in G1 (*Top Right* triangle map) vs. late anaphase (*Bottom Left* triangle map). Black arrowheads point at contact variations adjacent to the rDNA loci. Blue to red color scale indicates contact increase on chr *C* with 2xrDNA relative to 1xrDNA. The linear distance between the two rDNA loci in *cis* is indicated on the schematic of chr *C*. (*C*) Quantifications of Hi-C contacts between rDNA-flanking regions on chr *C* (dashed outline in the top triangle maps in panel *B*), as described in Fig. 3*B*. Relative contact reduction in anaphase (gray) compared to G1 (blue) is indicated for each strain with: one, two, and non-rDNA–containing proximal or distal locus.

investigated using microscopy, showing a high degree of structural conformity between 1xrDNA and 2xrDNA strains.

Design of the Megachromosome with twin rDNA Arrays and Their Genome (In)stability. Prior works on rDNA have employed interspecies hybrids to address if any differential stability of this locus in different yeasts (48–50). Most of these studies observed a uniparental loss of rDNA genes, a relevant example is the hybrid (50) between *S. cerevisiae* and *Saccharomyces eubayanus* in which the latter's locus collapsed completely whereas the one of *S. cerevisiae* remained full sized. Therefore, we reasoned that only by using two native and sequence-identical rDNA arrays located at different positions along the chromosome we could truly evaluate the position effect on their structure and stability.

The ectopic (*CEN*-proximal) location for rDNA megatransplantation corresponds to a chromosome fusion site, specifically the right and left ends of chr *XV* and chr *IV*, respectively. Given that these regions were initially subtelomeric, which typically lack essential genes, we reasoned that they would be "insensitive-to-insertion" (safe harbor) sites for the huge rDNA locus. Finally, the two loci in *cis* conserved the WT transcriptional orientation (*TEL*-to-*CEN*). Our results show a consistent reduction in size of the *CEN*-distal locus compared to the proximal counterpart. This peculiar size readjustment appears to be Sir2 dependent (*SI Appendix*, Fig. S3*E*), suggesting that the transcriptional activity—a major mechanism responsible for the rDNA gene array stability—at the two loci may be different. We speculate that the *CEN*-distal locus, which has native flanking sequences, is the predominantly transcribed locus and is therefore more prone to rapid size adjustments. In addition, the modest increase in *SIR2* transcription in the strains with a surplus of rDNA genes is consistent with the model proposed by Iida et al. (51), in which the limiting UAF (upstream activator factor for RNA polymerase I) complex was found to regulate rDNA copy homeostasis by modulating *SIR2* expression. In our specific case, the excess of rDNA genes (originating from the duplication of the rDNA array) would be expected to titrate the UAF complex away from p*SIR2*, leading to an increase in *SIR2* expression. Consequently, the increased level of Sir2 would then be able to compensate for the excess of rDNA copy number by silencing more rDNA genes, thus explaining the observed homeostasis in the rRNA level. Although this model can explain the size adjustment of the rDNA array, the question as to how rDNA-related factors work together to selectively maintain gene copy number at one locus in respect to the other remains open.

Nucleolus as a Phase Condensate. We found that the yeast rDNA readily forms a single nucleolus, independent of i) position in the genome (homologous or heterologous chromosomes) (35), ii) number of loci per chromosome (single or twin), and iii) rDNA array repeat size. These results are in full agreement with both nucleolar models proposed: LLPS and PPPS (5, 9), which envision that the intrinsic biochemical properties of the rDNA are the major driving forces for nucleolar assembly that can act over very long genomic distances.

Potential Consequences of a Twin-Colinear Organization of the rDNA Loci. Comparative evolutionary analyses of rDNA loci suggested that selective pressure may act to preserve specific characteristics (such as structure, number, and position) of these highly repetitive loci in eukaryotes. Here, we found that placing two rDNA loci in *cis* increases the rate of meiotic lethality (*SI Appendix*, Fig. S5 *A* and *B*), possibly due to mispairing of the homologous chromosomes driven by the 4 rDNA loci, which may facilitate abnormal recombination events and disrupt the rDNA-flanking regions (*SI Appendix*, Fig. S5*C*). We speculate that the misaligned chromatids can undergo unequal crossing-over, resulting in increased frequency of nonreciprocal exchange of genetic information (or gene conversion) and concomitant spore lethality. Our current model suggests that a high meiotic fitness cost is associated with multicolinear repeated loci, and this would be predicted to ultimately be purged from a sexual population. To support this model further, meiotic (in)stability of the two loci and evaluation of chromosomal rearrangements in viable spores remain to be investigated.

In addition, the extra copy of the rDNA locus appears to affect the metabolic response caused by early stages of nutrient consumption, which would initially induce cells in log-phase to exit this fast-growing phase, and enter a slow-growth period (diauxie) and eventually arrest. Our transcriptomic data suggest that the surplus of rDNA genes triggers a premature response to early nutrient deprivation, such as low glucose and phosphate levels (early signs that precede starvation). Second, we observed that the growth of these strains more closely resembles a classic growth curve that lacks the diauxic pattern typical of *S. cerevisiae* in rich medium (*SI Appendix*, Fig. S2*B* shows that the 2xrDNA strains saturate at a slightly higher cell density (A_{600}) than the 1xrDNA strains). However, the significance of this latter result was difficult to assess definitively due to high variability between isolates as well as the variability in length of the rDNA arrays.

Our transcriptomic data suggest that the 2xrDNA cells seemingly ignore signals that normally lead to diauxie. We hypothesize that the surplus of rDNA genes becomes a metabolic burden when cells need to rapidly enter into a mode that requires the strategic allocation of diminishing resources. We refer to this as the "relentless growth" model in which the signals responded to by normal cells to confer diauxie are bypassed by the cells with an excess of rDNA. This intriguing model requires further testing to better understand the chromatin status at the rDNA, the dynamics of rRNA transcription, as well as the transcriptomic and metabolic changes at different growth stages, including the return to growth of quiescent cells. In conclusion, we speculate that selective pressure acts to maintain rDNA repeat number within an effective "optimal range" to ensure that rRNA levels can be readily tuned in response to environmental changes. More generally, we term this potential fitness defect "paralogous *cis*-rDNA interference," whereby placement of two repeated and identical sequences in *cis* may cause interference with their function and ultimately lead to the loss of one locus.

These findings are noteworthy in the context of large-scale genome engineering, that, in our case, was implemented to address the structural evolution of gene arrays. Here, we have presented the living evidence of a chromosome configuration with two rDNA loci that coexist on the same chromosomal arm and found unexpectedly distinct rates of stability according to their relative locations on the chromosome. It appears that in the context of two *cis* loci, the array closer to the *CEN* is maintained stably relative to the distal twin. Given that our experimental design is confined to two chromosomal locations, additional experiments of genome editing to relocate either the *CEN* or the rDNA are required to validate this *CEN*-proximity effect. Nevertheless, our data suggest a potentially unique interplay between genome position and stability rate at least in the case of highly transcribed gene arrays.

Materials and Methods

Strains and Culture Conditions. All strains used in this study are listed in *SI Appendix*, Table S1, and they are derived from BY4741 and BY4742 (52) by transformation events. Deletion of the entire open-reading frame of *SIR2* gene

was performed using the CRISPR-Cas9 with a single gRNA and a ~1 kb-long repair donor generated by fusion PCR on *SIR2*-flanking sequences. The thermosensitive mutation in *CDC15* (*cdc15-2* ts) was introduced with CRISPR-Cas9. Oligos used in this study are listed in *SI Appendix*, Table S4.

Strains were grown in rich medium (YPD [yeast extract peptone dextrose] : 1% bacto peptone (Difco), 1% bacto yeast extract (Difco) and 2% glucose; YPG [yeast extract peptone glycerol] : 1% bacto peptone (Difco), 1% bacto yeast extract (Difco), and 3% glycerol) or in synthetic complete medium (SC [synthetic complete] : 0.67% yeast nitrogen base without amino acids (Difco), supplemented with a mix of amino acids and 2% glucose). The cells were grown at either 30 °C or 24 °C, the latter corresponds to the permissive temperature of the conditional thermosensitive mutant *cdc15-2* [see also methods in Lazar-Stefanita et al. (45)].

Serial Dilution Assay and Growth Curves. Yeast cultures from independent isolates of $n = 16$ WT rDNA (BY4741), $n = 3$ rDNA *CEN* distal (JL411), $n = 3$ rDNA *CEN* proximal (JL665), and $n = 3$ rDNA *CEN* proximal and distal (LS71) strains were grown in YPD liquid medium at 30 °C to saturation. For serial dilution assay, yeast cultures in stationary phase were diluted to an optical density (OD) $A_{600} = 0.1$ and serially diluted (1:10) in sterile water and then spotted on different media (YPD, YPG, and SC) and incubated at different temperatures (30 °C and 37 °C) for 2 d. For growth curves, yeast cultures in stationary phase were diluted in fresh YPD medium to $A_{600} = 0.05$, 200 µL was transferred to 96-well plates, and every minute the BioTek Eon microplate spectrophotometer was programmed to shake the plate and measure the A_{600} for a total of 24 h at 30 °C. A_{600} values were imported in GraphPad Prism version 9 for Mac OS (GraphPad Software, San Diego, California USA, www.graphpad.com) and used to calculate mean and SD for each isolate of each strain. Doubling time was calculated using the slope of the growth curves.

rDNA Megablock Engineering. A CRISPR-Cas9-based method was used to promote during the cut-and-paste rDNA locus relocation from the native location (flanked by chromosome *XII* sequence) to an ectopic position generated by fusing *TEL 15R* and *TEL 4L*. The method was performed as described by Luo et al. (36), except that two gRNAs cut the flanking regions of rDNA locus and the third gRNA cuts at the new ectopic insertion site. In addition, three donor templates were generated by fusion PCR, they include: i) a donor template to rejoin the ends of the native locus upon rDNA deletion, ii) a donor template for bridging the left flanking region of the rDNA locus to its new target location, and iii) a donor template for bridging the right flanking region of rDNA locus to its new target location. rDNA translocation was verified by PCR with primer pairs designed outside the newly formed chromosome junctions. Guide RNAs and PCR primers are listed in *SI Appendix*, Table S4.

PFGE and Dual-Color Southern Blot. Chromosomes from stationary yeast cell cultures were prepared in agar molds using the Certified Megabase Agarose (Bio-Rad CAT. 1613108), and PFGE was carried out as previously described, with running conditions recommended for either *S. cerevisiae* or *Saccharomyces pombe* chromosomes. Specifically, megachromosomes were separated on a 0.8% agar gel in 1× TAE (Tris acetate ethylene diamine tetra-acetic acid) at 14°C. Run time was ~72 h at 2V/cm with switch time of 20 to 30 min at an included angle of 106° (36). DNA size markers used were the *S. pombe* chromosomal DNA (Bio-Rad CAT. 170-3633) and the *Hansenula wingei* chromosomal DNA (Bio-Rad CAT. 170-3667).

Method for chromosome digestion. Prior to the BamHI (NEB CAT. R0136L) incubation, agar plugs were equilibrated 1× Buffer3.1 (NEB) for 24 h at 4 °C. BamHI digest was carried out for 24 h at 37 °C in ~500 µL final volume consisting of: ~100 mg agar, 50 µL 10× restriction buffer, and 10 µL BamHI enzyme (200 U). Agar molds treated with BamHI were then used for the PFGE and Southern blot.

The protocol for dual-color Southern blotting was optimized based on a previous study by Zavala et al. (53). Following electrophoresis of BamHI-digested agar plugs, the gel was washed in depurination solution (0.25 M HCl) for 20 min, denaturation solution (0.5 M NaOH, 1.5 M NaCl) for 60 min, and neutralization solution (0.5 M Tris, 1.5 M NaCl pH 7.5) for 30 min. Chromosomes were transferred by capillarity to a nylon membrane (Pall® 60208 Biodyne™ B Membrane, Pore Size 0.45 µm CAT. 60208) using 10X SSC buffer (20× SSC: 1.5 M NaCl, 0.3 M sodium citrate pH 7) for 72 h. After transfer, the membrane was washed with 2× SSC for 5 min and baked at 80 °C for 30 min. Prehybridization and hybridization steps were performed at 50 °C in ULTRAhyb™ Ultrasensitive Hybridization Buffer (Invitrogen Ambion CAT. AM8670). PCR products (~1.1 kb-long flanking unique sequences on either side of each rDNA locus) were labeled using Klenow Fragment exo- (NEB CAT. M0212L) with either Biotin-16-dUTP (Roche CAT. 11093070910) or Digoxigenin-11-dUTP alkali-stable (Roche CAT. 11093088910) at 37 °C for 1 h. Oligos used for making DNA probes are listed in *SI Appendix*, Table S4. Labeled DNA probes were cleaned up using Zymo-Spin I Columns (Zymo Research CAT. C1003-50), denatured at 95 °C for 5 min, and ~300 ng of each was used for each hybridization experiment. The blot was washed twice with 2× SSPE buffer (20× SSPE Buffer: 0.02 M EDTA and 2.98 M NaCl in 0.2 M phosphate buffer pH 7.4; Sigma-Aldrich CAT. S2015) for 5 min at room temperature; twice with 2× SSPE, 1% SDS for 30 min at 55 °C; and twice with 0.1× SSPE for 15 min at 55 °C. Blot was incubated in Blocking buffer Odyssey (LI-COR® CAT. 927-40000) in 1× Tris-Buffered Saline with 0.1% Tween 20 and 1% SDS for 3 h at room temperature.

The membrane was washed with 1× TBST for 5 min and incubated for 1 h at room temperature with rabbit anti-DIG antibody (working concentration 1:2,500 in Blocking buffer Odyssey; ABfinity™ Rabbit Monoclonal, CAT. 700772). The primary antibody solution was washed out three times with 1× TBST for 15 min at room temperature. The membrane was incubated in the secondary antibody solution (working concentration 1:10,000 in Blocking buffer Odyssey): Licor IRDye® 800CW Streptavidin, 0.5 mg (CAT. 926-32230), and LIRDye® 680RD Goat anti-Rabbit IgG (H + L), 0.5 mg (CAT. 926-68071), for 30 min at room temperature. The secondary antibody solution was discarded and the membrane was washed three times with 1× TBST for 15 min at room temperature before imaging acquisition using LI-COR Odyssey® Imager.

Mating Type Switching, Sporulation, and Tetrad Dissection. For mating type switch, we used the same reagents and protocol described by Zhang et al. (34). A detailed protocol for sporulation and tetrad dissection of yeast with fused chromosomes was described by Luo et al. (36).

RNA Extractions. Total RNA was extracted from 3 independent isolates of $n = 16$ WT rDNA (BY4741), $n = 3$ rDNA *CEN* distal (JL411), $n = 3$ rDNA *CEN* proximal (JL665), and $n = 3$ rDNA *CEN* proximal and distal (LS71) strains. Approximately 2×10^8 cells were harvested from log-phase cultures (1.5 to 2×10^7 cells/ml) grown in YPD medium at 30 °C. Cell pellets were washed in RNase-free water and resuspended in RNA lysis buffer (50 mM Tris-HCl pH 8, 100 mM NaCl). The cells were lysed mechanically using acid-washed glass beads (Sigma-Aldrich CAT. G8772-100G) at 4 °C. The RNA was extracted by phenol:chloroform:isoamylalcohol (ThermoFisherScientific CAT. 15593) and ethanol precipitated. Extractions were treated with DNaseI (Agilent CAT. 600031) for 1 h at 37 °C and RNA quality was verified by agarose gel in 1× TAE.

RT-qPCR. The above total RNA extractions were serial diluted (1:10/100/1,000) and used for RT-qPCR reactions with gene-specific oligos (rRNA: 18S, 25S, ETS1 [external transcribed spacer 1] ; mRNA: *TAF10*, *UBC6*). The reverse transcriptase (RT) reaction was performed according to the manufacturer's protocol SuperScript™ IV RT (Invitrogen CAT. 18090050). Successively, quantitative PCR was performed using either the LightCycler® 480 SYBR Green I Master (Roche CAT. 04887352001) or One-Step PrimeScript™ III RT-qPCR Mix (Takara CAT. RR600A) with multiplexed fluorescent probes (fluorescein, FAM; hexachlorofluorescein, HEX), with the standard amplification protocol with 45 cycles in a multiwell PCR plate 384. Ct values for each replicate were imported in GraphPad Prism version 9 for Mac OS (GraphPad Software, San Diego, California USA, www.graphpad.com) and used to calculate mean and SD for each gene in each strain. Raw Ct values for each gene can be found in Dataset S1.

RNA Library Preparation, Sequencing, and Analysis. Stranded total RNA-seq libraries were prepared with the QIAseq stranded RNA library kit (Qiagen, CAT. 180743) following the manufacture's recommendations using dual-indexing primers. Additionally, the input total RNA was first processed with the QIAseq FastSelect rRNA Yeast kit to remove cytoplasmic and mitochondrial rRNA (Qiagen, CAT. 334215). Library quality was assessed using the ZAG 110 dsDNA kit on (Agilent, CAT. ZAG-110-5000) and run on the ZAG DNA analyzer system (Agilent). Libraries were then sequenced on an Illumina NextSeq 500 using the 75-cycle high output in paired-end mode (Illumina, CAT. 20024906).

Differential gene analysis **(**Dataset S2**).** RNA sequencing analysis was performed as previously described (54) using kallisto/sleuth suite with minor modifications. Briefly,

reads were processed by Illumina barcode and quality trimmed with Trimmomatic (55) and quality assessed with FastQC (56). Next, the reads were aligned using the pseudo-alignment program kallisto to the reference S288C genome (57), with annotations supplied with a gtf file containing all annotated RNAs in stranded paired-end mode (options, --genomebam --gtf --fr-stranded). The output of Kallisto was then used for data analysis in Sleuth (58). Volcano plots were generated using the Walds test false discovery rate-adjusted *P* value ($P < 0.01$) and log2 fold change ($-2 > \text{Log2FC} > 2$).

Cell Cycle Synchronization. For both imaging and Hi-C experiments, yeast cells, carrying either a single rDNA locus (LS88, LS95) or two rDNA loci in *cis* (LS90, LS103), were synchronized in either G1 with alpha factor (Zymo Research, CAT. Y1001), or in late anaphase, using the thermosensitive mutant *cdc15-2*.

Method for G1 synchronization (LS88 and LS90). Cells were grown to saturation in 5 mL SC medium at 30 °C; the next day, the cells were subcultured in 150 mL fresh SC medium (OD, $A_{600} = 0.5$) for 2 h 30 min at 30 °C and then alpha factor was added (final concentration: 25 μM) and cultures were incubated for additional 2 h 30 min at 24 °C before imaging and formaldehyde cross-link.

Method for late anaphase synchronization (LS95 and LS103). Cells were grown to saturation in 5 mL SC medium at 24 °C; the next day, they were subcultured in 150 mL fresh SC medium ($A_{600} = 0.5$) and grown for 5 h at 24 °C and then the temperature was switched to 37 °C (nonpermissive condition) and incubated for additional 3 h before imaging and formaldehyde cross-link.

The quality of G1 and anaphase synchronizations was visually monitored by microscopy hourly. For microscopy, small aliquots (~1 to 2 mL synchronized cultures) were spooned down at 3,000 g for 3 min and fixed in ethanol 70%; whereas, the remaining cultures were fixed with formaldehyde for Hi-C library preparation (see below).

Protein Tagging and Imaging of the Nucleolus. The cell cycle reorganization of the nucleolus within the nucleus was monitored using fluorescently tagged proteins at their endogenous C terminus. Nuclear envelope was labeled with either mCherry (*NIC96::mCherry*) or mScarlet (*NUP49::mScarlet*), while the nucleolus with GFP (*NOP10::EGFP*) as described by Zhang et al. (34) (see also strain genotype in *SI Appendix*, Table S1). Imaging was performed on the EVOS M7000 microscope using the Olympus X-APO 100 Oil, 1.45NA/WD 0.13 mm (Oil) objective. Images were acquired as Z-stacks and visualized as max intensity projections using ImageJ (59).

Hi-C Library Preparation and Data Analysis. Hi-C libraries (*SI Appendix*, Table S3) were prepared from yeast cells harvested from either log phase or cell cycle synchronized cultures (see above protocols for cell synchronizations). Methods for yeast Hi-C library preparation and data analysis were performed as previously described by Lazar-Stefanita et al. (45, 46). Briefly, Hi-C reads were aligned using Bowtie 2 (60) and processed using command lines based on HiCLib tool developed in the Mirny lab (61). Normalized contact maps [sequential component normalization (62)] were 5 kb-binned and were plotted using MatLab R2018 (The MathWorks, Inc., Natick, Massachusetts, United States).

The Hi-C assay resulted crucial to validate the transplantation of the rDNA locus. We found that among the potential candidates–that were PCR positive for the rDNA transplantation–only one isolate had the entire locus relocated that resulted in the actual repositioning of the rDNA boundary from the native location (*CEN*-distal: 2.75 Mb from the active centromeric sequence, *CEN15,* and 0.6 Mb from the nearest telomeric sequence, *TEL12R*) to the new ectopic position at the fusion junction between the left arm of former chromosome *XV* and the right arm of former chromosome *IV* (*CEN*-proximal: 0.75 Mb from *CEN15* and 2.52 Mb from *TEL12R*). Of note, in the isolates that were false positives by PCR for the rDNA megablock transplantation, the chromosome boundary formed by this locus remained at the original location (*CEN*-distal) as expected.

The Hi-C maps were used to evaluate the strength of each rDNA boundary in function of their distance from the *CEN* and locus number (single vs. double) across megachromosome *C*. For this analysis, we first reasoned that the chromosome boundaries observed at the location of the rDNA loci on the 2D maps are "visual artifacts" due to the combination of different structural characteristics at this locus. Indeed, the highly repetitive nature and the formation of a subnuclear compartment (nucleolus) appear to lower the contact frequency between the rDNA-flanking regions. Along the same lines, we also expected that differences in structure and/or size between rDNA loci would have an effect on the strength of the correspondent chromosome boundaries. In other words, the bigger the rDNA locus ("bulkier" the nucleolus), the lower the contact frequency between its flanking sequences, and therefore the stronger the boundary. To compare between the *CEN*-proximal and *CEN*-distal rDNA boundaries, located in single (JL411 and JL665) or double copy (LS71 C1 to C3) on megachromosome *C*, we used normalized Hi-C contact maps (5 kb-binned) to quantify interactions between 500 kb-long regions–corresponding to the upstream *CEN* proximal locus and to the downstream *CEN* distal locus (see blue rectangles on chr *C* maps in Fig. 3*A*)–and the 1.9 Mb intervening region between the two loci. Spread point plots, where each point corresponds to total contacts made by each 5 kb bin, were generated for each rDNA boundary using Matlab. *P* values were calculated using the Kolmogorov–Smirnov test (K–S test) function in MATLAB 2018a (The MathWorks, Inc., Natick, Massachusetts, United States).

Log2 ratios of Hi-C contact maps were used for their pairwise comparison, and the contact probability decay in function of the genomic distance, $p(s)$, was computed to assess the status of the chromatin fiber. Both these analyses were performed as previously described by Lazar-Stefanita et al. (45, 46).

Data, Materials, and Software Availability. Genome-wide and RNA sequencing files were deposited at the NCBI database as FASTQ files. See BioProject accession number PRJNA847233 for the SRA data.

ACKNOWLEDGMENTS. We acknowledge all members of Boeke lab for their assistance and Liam Holt for helpful discussions. We thank Aleksandra Wudzinska and Gregory W. Goldberg for their assistance and helpful comments on the manuscript. This work was supported by NSF grants MCB-1616111 and MCB-1921641 and NIH grant RM1HG009491 to J.D.B.

Author affiliations: [a]Institute for Systems Genetics, NYU Langone Health, New York, NY 10016; [b]Department of Biochemistry and Molecular Pharmacology, NYU Langone Health, New York, NY 10016; [c]Vilcek Institute of Graduate Biomedical Sciences at NYU School of Medicine, New York, NY 10016; and [d]Department of Biomedical Engineering, NYU Tandon School of Engineering, Brooklyn, NY 11201

Author contributions: L.L.-S. and J.D.B. conceptualized the research; L.L.-S., J.L., M.A.B.H., and W.Z. designed research; L.L.-S., J.L., M.A.B.H., and W.Z. performed research; L.L.-S. contributed new reagents/analytic tools; L.L.-S. and M.A.B.H. analyzed data; and L.L.-S. and J.D.B. wrote the paper.

1. E. O. Long, I. B. Dawid, Repeated genes in eukaryotes. *Annu. Rev. Biochem.* **49**, 727–764 (1980).
2. T. D. Petes, Yeast ribosomal DNA genes are located on chromosome XII. *Proc. Natl. Acad. Sci. U.S.A.* **76**, 410–414 (1979).
3. J. E. Sylvester *et al.*, The human ribosomal RNA genes: Structure and organization of the complete repeating unit. *Hum. Genet.* **73**, 193–198 (1986).
4. J. R. Warner, The economics of ribosome biosynthesis in yeast. *Trends Biochem. Sci.* **24**, 437–440 (1999).
5. D. L. J. Lafontaine, J. A. Riback, R. Bascetin, C. P. Brangwynne, The nucleolus as a multiphase liquid condensate. *Nat. Rev. Mol. Cell Biol.* **22**, 165–182 (2021).
6. T. Pederson, The Nucleolus. *Cold Spring Harb. Perspect. Biol.* **3**, a000638 (2011).
7. M. Thiry, D. L. J. Lafontaine, Birth of a nucleolus: The evolution of nucleolar compartments. *Trends Cell Biol.* **15**, 194–199 (2005).
8. J. C. Hansen, K. Maeshima, M. J. Hendzel, The solid and liquid states of chromatin. *Epigenet. Chromatin* **14**, 50 (2021).
9. J. Lawrimore *et al.*, The rDNA is biomolecular condensate formed by polymer–polymer phase separation and is sequestered in the nucleolus by transcription and R-loops. *Nucleic Acids Res.* **49**, 4586–4598 (2021).
10. M. Feric *et al.*, Coexisting liquid phases underlie nucleolar subcompartments. *Cell* **165**, 1686–1697 (2016).
11. F. Erdel, K. Rippe, Formation of chromatin subcompartments by phase separation. *Biophys. J.* **114**, 2262–2270 (2018).
12. F-M. Boisvert, S. van Koningsbruggen, J. Navascués, A. I. Lamond, The multifunctional nucleolus. *Nat. Rev. Mol. Cell Biol.* **8**, 574–585 (2007).
13. D. Hernandez-Verdun, Assembly and disassembly of the nucleolus during the cell cycle. *Nucl. Austin Tex* **2**, 189–194 (2011).
14. R. Srivastava, R. Srivastava, S. H. Ahn, The epigenetic pathways to ribosomal DNA silencing. *Microbiol. Mol. Biol. Rev. MMBR* **80**, 545–563 (2016).
15. S. L. French, Y. N. Osheim, F. Cioci, M. Nomura, A. L. Beyer, In exponentially growing Saccharomyces cerevisiae Cells, rRNA synthesis is determined by the summed RNA polymerase I loading rate rather than by the number of active genes. *Mol. Cell. Biol.* **23**, 1558–1568 (2003).
16. L. J. Weider *et al.*, The functional significance of ribosomal (r)DNA variation: Impacts on the evolutionary ecology of organisms. *Annu. Rev. Ecol. Evol. Syst.* **36**, 219–242 (2005).
17. T. Kobayashi, D. J. Heck, M. Nomura, T. Horiuchi, Expansion and contraction of ribosomal DNA repeats in Saccharomyces cerevisiae: Requirement of replication fork blocking (Fob1) protein and the role of RNA polymerase I. *Genes Dev.* **12**, 3821–3830 (1998).

18. J. C. Sanchez *et al.*, Defective replication initiation results in locus specific chromosome breakage and a ribosomal RNA deficiency in yeast. *PLoS Genet.* **13**, e1007041 (2017).
19. T. Kobayashi, A. R. D. Ganley, Recombination regulation by transcription-induced cohesin dissociation in rDNA repeats. *Science* **309**, 1581–1584 (2005).
20. T. Kobayashi, M. Sasaki, Ribosomal DNA stability is supported by many 'buffer genes'–introduction to the Yeast rDNA Stability Database. *FEMS Yeast Res.* **17**, fox001 (2017).
21. D. Salim, J. L. Gerton, Ribosomal DNA instability and genome adaptability. *Chromosome Res.* **27**, 73–87 (2019).
22. S. Gottlieb, R. E. Esposito, A new role for a yeast transcriptional silencer gene, SIR2, in regulation of recombination in ribosomal DNA. *Cell* **56**, 771–776 (1989).
23. S. Garcia, A. Kovařík, A. R. Leitch, T. Garnatje, Cytogenetic features of rRNA genes across land plants: Analysis of the Plant rDNA database. *Plant J.* **89**, 1020–1030 (2017).
24. J. Sochorová, S. Garcia, F. Gálvez, R. Symonová, A. Kovařík, Evolutionary trends in animal ribosomal DNA loci: introduction to a new online database. *Chromosoma* **127**, 141–150 (2018).
25. B. M. Robicheau, E. Susko, A. M. Harrigan, M. Snyder, Ribosomal RNA genes contribute to the formation of pseudogenes and junk DNA in the human genome. *Genome Biol. Evol.* **9**, 380–397 (2017).
26. E. Proux-Wéra, K. P. Byrne, K. H. Wolfe, Evolutionary mobility of the ribosomal DNA array in yeasts. *Genome Biol. Evol.* **5**, 525–531 (2013).
27. D. D. Brown, P. C. Wensink, E. Jordan, A comparison of the ribosomal DNA's of Xenopus laevis and Xenopus mulleri: the evolution of tandem genes. *J. Mol. Biol.* **63**, 57–73 (1972).
28. T. H. Eickbush, D. G. Eickbush, Finely orchestrated movements: Evolution of the ribosomal RNA genes. *Genetics* **175**, 477–485 (2007).
29. J. G. Gibbons, A. T. Branco, S. A. Godinho, S. Yu, B. Lemos, Concerted copy number variation balances ribosomal DNA dosage in human and mouse genomes. *Proc. Natl. Acad. Sci.* **112**, 2485–2490 (2015).
30. T. D. Petes, D. Botstein, Simple Mendelian inheritance of the reiterated ribosomal DNA of yeast. *Proc. Natl. Acad. Sci.* **74**, 5091–5095 (1977).
31. M. Nomura, Y. Nogi, M. Oakes, *Transcription of rDNA in the Yeast Saccharomyces cerevisiae* (Landes Bioscience, 2013), (January 13, 2021).
32. Y.-H. Kim *et al.*, Chromosome XII context is important for rDNA function in yeast. *Nucleic Acids Res.* **34**, 2914–2924 (2006).
33. N. Dvorkin, M. W. Clark, B. A. Hamkalo, Ultrastructural localization of nucleic acid sequences in Saccharomyces cerevisiae nucleoli. *Chromosoma* **100**, 519–523 (1991).
34. W. Zhang *et al.*, Engineering the ribosomal DNA in a megabase synthetic chromosome. *Science* **355**, eaaf3981 (2017).
35. C. Hult *et al.*, Enrichment of dynamic chromosomal crosslinks drive phase separation of the nucleolus. *Nucleic Acids Res.* **45**, 11159–11173 (2017).
36. J. Luo, X. Sun, B. P. Cormack, J. D. Boeke, Karyotype engineering by chromosome fusion leads to reproductive isolation in yeast. *Nature* **560**, 392–396 (2018).
37. Q. Ju, J. R. Warner, Ribosome synthesis during the growth cycle of Saccharomyces cerevisiae. *Yeast* **10**, 151–157 (1994).
38. J. S. Smith, J. D. Boeke, An unusual form of transcriptional silencing in yeast ribosomal DNA. *Genes Dev.* **11**, 241–254 (1997).
39. K. Merz *et al.*, Actively transcribed rRNA genes in S. cerevisiae are organized in a specialized chromatin associated with the high-mobility group protein Hmo1 and are largely devoid of histone molecules. *Genes Dev.* **22**, 1190–1204 (2008).
40. T. Kobayashi, T. Horiuchi, P. Tongaonkar, L. Vu, M. Nomura, SIR2 regulates recombination between different rDNA repeats, but not recombination within individual rRNA genes in yeast. *Cell* **117**, 441–453 (2004).
41. J. Dekker, K. Rippe, M. Dekker, N. Kleckner, Capturing chromosome conformation. *Science* **295**, 1306–1311 (2002).
42. E. Lieberman-Aiden *et al.*, Comprehensive mapping of long-range interactions reveals folding principles of the human genome. *Science* **326**, 289–293 (2009).
43. A. Amon, A decade of Cdc14–A personal perspective. *FEBS J.* **275**, 5774–5784 (2008).
44. A. Clemente-Blanco, Nucleolar condensation: A new mechanism to control mitotic exit. *Curr. Biol.* **27**, R1220–R1222 (2017).
45. L. Lazar-Stefanita *et al.*, Karyotype engineering reveals spatio-temporal control of replication firing and gene contacts. *Cell Genomics* **2**, 100163 (2022).
46. L. Lazar-Stefanita *et al.*, Cohesins and condensins orchestrate the 4D dynamics of yeast chromosomes during the cell cycle. *EMBO J.* **36**, 2684–2697 (2017).
47. L. H. Hartwell, J. Culotti, J. R. Pringle, B. J. Reid, Genetic control of the cell division cycle in yeast. *Science* **183**, 46–51 (1974).
48. J. L. Gordon, K. H. Wolfe, Recent allopolyploid origin of Zygosaccharomyces rouxii strain ATCC 42981. *Yeast* **25**, 449–456 (2008).
49. V. L. Louis *et al.*, Pichia sorbitophila, an interspecies yeast hybrid, reveals early steps of genome resolution after polyploidization. *G3 Bethesda Md* **2**, 299–311 (2012).
50. Y. Nakao *et al.*, Genome sequence of the lager brewing yeast, an interspecies hybrid. *DNA Res. Int. J. Rapid Publ. Rep. Genes Genomes* **16**, 115–129 (2009).
51. T. Iida, T. Kobayashi, RNA polymerase I activators count and adjust ribosomal RNA gene copy number. *Mol. Cell* **73**, 645–654.e13 (2019).
52. C. B. Brachmann *et al.*, Designer deletion strains derived from Saccharomyces cerevisiae S288C: A useful set of strains and plasmids for PCR-mediated gene disruption and other applications. *Yeast Chichester Engl.* **14**, 115–132 (1998).
53. A. G. Zavala, A. S. Kulkarni, E. A. Fortunato, A dual color southern blot to visualize two genomes or genic regions simultaneously. *J. Virol. Methods* **198**, 64–68 (2014).
54. D. M. Truong, J. D. Boeke, Resetting the yeast epigenome with human nucleosomes. *Cell* **171**, 1508–1519.e13 (2017).
55. A. M. Bolger, M. Lohse, B. Usadel, Trimmomatic: A flexible trimmer for Illumina sequence data. *Bioinformatics* **30**, 2114–2120 (2014).
56. N. L. Bray, H. Pimentel, P. Melsted, L. Pachter, Near-optimal probabilistic RNA-seq quantification. *Nat. Biotechnol.* **34**, 525–527 (2016).
57. S. R. Engel *et al.*, The reference genome sequence of Saccharomyces cerevisiae: Then and now. *G3 Bethesda* **4**, 389–398 (2014).
58. H. Pimentel, N. L. Bray, S. Puente, P. Melsted, L. Pachter, Differential analysis of RNA-seq incorporating quantification uncertainty. *Nat. Methods* **14**, 687–690 (2017).
59. C. A. Schneider, W. S. Rasband, K. W. Eliceiri, NIH Image to ImageJ: 25 years of image analysis. *Nat. Methods* **9**, 671–675 (2012).
60. B. Langmead, S. L. Salzberg, Fast gapped-read alignment with Bowtie 2. *Nat. Methods* **9**, 357–359 (2012).
61. M. Imakaev *et al.*, Iterative correction of Hi-C data reveals hallmarks of chromosome organization. *Nat Methods* **9**, 999–1003 (2012).
62. A. Cournac, H. Marie-Nelly, M. Marbouty, R. Koszul, J. Mozziconacci, Normalization of a chromosomal contact map. *BMC Genomics* **13**, 436 (2012).